Post-LGM glacial retreat drives aggradation in the interiors of the Kashmir Himalaya

Saptarshi Dey, IIT Gandhinagar, Gandhinagar-382355, India. saptarshi.dey@iitgn.ac.in

Naveen Chauhan, Physical Research Laboratory, Ahmedabad- 380009, India. chauhan@prl.res.in

Anushka Vasistha, IIT Gandhinagar, Gandhinagar-382355, India. anushka.vashistha@iitgn.ac.in

Vikrant Jain, IIT Gandhinagar, Gandhinagar-382355, India. vjain@iitgn.ac.in

Corresponding author email: saptarshi.dey@iitgn.ac.in

6/24/2021

Statement: This work was submitted to Geomorphology in January 2021. This is a non-peer reviewed preprint submitted to EarthArXiv. If accepted, 'peer-reviewed publication DOI' link will be available on this webpage.

Post-LGM glacial retreat drives aggradation in the interiors of the Kashmir Himalaya

Saptarshi Dey, Naveen Chauhan, Anushka Vasistha, and Vikrant Jain

Abstract

Understanding the response of glaciated catchments to climate change is fundamental for assessing sediment transport from the high-elevation, semi-arid to arid sectors in the Himalaya to the foreland basin. The fluvioglacial sediments stored in the semi-arid Padder valley in the Kashmir Himalaya record valley aggradation during ~19-11 ka. We relate the valley aggradation to increased sediment supply from the deglaciated catchment during the glacial-to-interglacial phase transition. Previously-published bedrock-exposure ages in the upper Chenab valley suggest ~180 km retreat of the valley glacier during ~20-15 ka. Increasing roundness of sand-grains and reducing mean grain-size from the bottom to the top of the valley-fill sequence hint about increasing fluvial transport with time and corroborate with the glacial retreat history. Our result also correlates well with late Pleistocene-early Holocene sediment aggradation observed across most Western Himalayan valleys. It highlights the spatiotemporal synchronicity of sediment transfer from the Himalayas triggered by climate change.

Keywords

Aggradation; deglaciation; Last Glacial Maximum; luminescence dating; Kashmir Himalaya.

1. Introduction

Understanding the role of past climate change on surface processes is essential to forecast how landscapes respond to global warming. For example, changes in temperature and precipitation can have a strong impact on weathering (Dosseto et al., 2015), surface runoff, and sediment transport from the mountain to the basin (e.g., Tucker and Slingerland, 1997; Bookhagen et al., 2005; Scherler et al., 2015). It is understood that global warming poses greater implications for high-mountain areas as it would trigger deglaciation and glacial retreat (e.g., Benn and Owen, 2002; Barnard et al., 2006; Eugster et al., 2016; Rashid et al., 2017). As a glacier retreats, it releases massive volumes of sediments in the subsequent drainage system as glacial outwash (e.g., Meigs et al., 2006; Smith et al., 2017).

Sediment transport from the Himalaya to the foreland basin over millennial timescales is suggested to be driven by climatic fluctuations such as glacial-interglacial phase transitions (e.g., Joussain et al., 2016) and intensified monsoon phases (e.g., Bookhagen et al., 2005; Dey et al., 2016). Present understanding of the climatic variations over 10^3-10^5-years timescales suggests that the climatic cycles are dependent on Earth's orbital parameters, such as eccentricity and orbital precision (Milankovich, 1941). While the eccentricity cycles over ~100 ka cause the glacial-interglacial cycles, the ~21-23 ka precision is suggested to be driving the monsoonal variations. Foreland-bound sediments are often transiently-stored within the river valleys and intermontane basins across the entire Himalayan orogen. These sediment archives help us examine the role of climatic fluctuations behind spatiotemporal variability in sediment flux (e.g., Bookhagen et al., 2006; Scherler et al., 2015; Dey et al., 2016; Dutta et al., 2018). Over the last couple of decades, many of the major Himalayan drainages and intermontane valleys have been studied to obtain sedimentological and chronological constraints on the transiently-stored valley-fills. The studies spanned throughout the entire Himalayan front- from the eastern Himalaya (e.g., Srivastava et al., 2009; Panda et al., 2020), the central Himalaya (e.g., Pratt Sitaula et al., 2004; Meetei et al., 2007; Singh et al., 2017) and the western Himalaya (e.g., Bookhagen et al., 2006; Suresh et al., 2007; Ray and Srivastava, 2010; Sinha et al., 2010; Dutta et al., 2012; Vassallo et al., 2015; Dey et al., 2016; Dutta et al., 2018). Interestingly, most studies have been conducted in humid to extreme-humid zones near the orographic front, where decoupling the glacial cycles and monsoon cycles are tricky. Continental oxygen isotope proxy (e.g., Wang et al., 2008) and Northern Hemisphere Summer Solar Insolation (NHSI) data (Huybers, 2006) suggest that the glacial-interglacial cycle and monsoon cycles broadly overlap with each other. Therefore, understanding the impact of monsoon variability and glaciation-deglaciation by assessing intermontane valley archives is often challenging. To decouple this situation and to study the role of glaciation-deglaciation in sediment transport, we must investigate sediment archives from arid to semi-arid sectors of the Himalaya, where rainfall is low (< 1 m/yr). Semi-arid to arid sectors of the western Himalaya are situated at higher elevations (> 3 km asl) in the north of the main orographic barrier formed by the Lesser and Higher Himalaya (Bookhagen and Burbank, 2010) (Fig.1). The high-elevation interiors of the western Himalaya show significant glacial coverage at present and in the geological past (Owen et al., 2008). In the last few years, studies have explored climatic and tectonic implications of valley-fills in arid interiors of the Himalaya (Srivastava et al., 2013; Blöthe et al., 2014; Kumar and Srivastava, 2017; Chahal et al., 2019). Some of the studies favored the role of deglaciation in transient aggradation of river valleys (e.g., Ray and Srivastava, 2010; Sharma et al, 2016; Kothyari et al., 2017). Still, the data is sparse, and the spatiotemporal synchronicity of climate-driven aggradation-incision cycles is yet to be tested.

In pursuit of a better understanding of the role of climate change in sediment transport in glaciated catchments, we investigated the aggraded sediments from the Padder valley in the Kashmir Himalaya (cf. Fig.1 for location). In this study, we combined detailed field observations on valley morphology, sedimentology, and sediment chronology to explore how sediment archives can record evidence of glacial retreat.

2. Geological background

The Padder valley is situated at the eastern margin of the Kishtwar tectonic window in the Kashmir Himalaya interiors at an elevation of ~1750-1760m above mean sea-level. The Kishtwar Window exposes the Lesser Himalayan duplex undergoing rapid exhumation at a rate of ~3 mm/yr since at least Quaternary (Gavillot et al., 2018). In the upstream, however, the Higher Himalayan crystalline and medium-high grade Higher Himalayan metasediments are exposed, which exhumes much slower (~0.2-0.4 mm/yr). The valley is drained by the Chenab River, which originates in the Lahaul-Spiti region of northern Himachal Pradesh, India and traverses ~350 km till it reaches the Padder valley. The 'U-shaped' Padder valley (Fig.2 inset) indicates glacial occupancy in the past. However, it is unknown at which time-period the glaciers came down below the 2-km elevation line above mean sea level (msl). Previous works suggest that the upper Chenab valley has been subjected to glacial advancement and retreat (Kulkarni et al., 2007; Eugster et al., 2016). Eugster et al., (2016) constrained the advancement of the Chenab valley glacier by ^{10}Be exposure ages from glacially-polished Higher Himalayan bedrock. In Fig.2, we portrayed the longitudinal elevation profile of the Chenab River and marked the temporal variations in glacial extent after Eugster et al., (2016). Around ~20 ka, the Chenab valley glacier was at ~2400m above msl (marked by point G1 in Fig.2), while about ~15 ka ago, the glacier was at ~4150m above msl (point G4 in Fig.2). Eugster et al., (2016) documents ~180 km glacial retreat towards upstream within a span of only 5-6 ka.

3. Methods

3.1. Field observation

The Padder valley records ~100m thick aggraded sediment sequence (Fig. 2 inset, 3b, 4a). The valley-fill sediments are re-incised by the Chenab River, and that has sculpted at least five terrace levels in the valley. Terraces (T1-T5) are classified according to their decreasing heights from the River (Fig. 3a). The River is still incising the valley-fill in the study area. The valley-fills are comprised of angular boulders, sub-rounded to rounded pebbles, sand of different sizes and shapes, and occasional silt layers (Fig.4). The boulders and pebbles are mostly of Higher Himalayan origin, as it represents rocks of Higher Himalayan gneisses and high-grade schists. However, the valley-fills are also punctuated by a series of coarse-grained angular debris units with a dominant Lesser Himalayan input characterized by Lesser Himalayan granites and quartzites. We propose that these angular, poorly-sorted 'debris' represents the hillslope sediment flux from the surrounding Lesser Himalayan units at the eastern margin of the Kishtwar Window. Overall, in the lower part of the aggradation sequence, the size of the clasts are bigger (sometimes more than a meter), and the clasts are less rounded (Fig.4b). But, as we go to the top of the sediment log, the clast-size reduces, and the clasts' roundness increases (Fig.4c). Near the top, the clasts are perfectly-rounded and polished (Fig.4d). Similar observations on grain-size and shapes are persistent with the finer fractions. Near the Chenab Riverbed, one ~3-4m thick sand layer is present, which has very well-sorted, moderately-rounded grains in it but lacks lamination.

3.2. Luminescence chronology

Luminescence dating is a widely-accepted method for assessment of sediment depositional ages across various depositional environments, including fluvial (e.g., Fuchs and Lang, 2001; Cunningham and Wallinga, 2012), glacial (e.g., Hu et al., 2015; Mehta et al., 2012), Aeolian (e.g., Lai et al., 2009; Kumar et al., 2017) and lacustrine (e.g., Fan et al., 2010; Long et al., 2011) settings. Optically stimulated luminescence dating (OSL) using quartz grains from fine-medium sand layers in the sediment archive is, therefore, a potent option to constrain timings of sediment aggradation. We sampled five samples from the medium sand layers (SD/P01-P05) and one sample from the fine sand layers (SD/P06) for OSL measurement. The sand from the same layers was further used for grain-size and grain-shape analysis.

All samples were collected in sealed galvanized iron pipes and opened only in subdued red light (wavelength ~650 nm) in the laboratory. The outer ~3 cm of each end of the pipes were discarded to avoid accidental exposure to sunlight during sample procurement. Quartz grains of 90-150 µm size fraction was extracted using standard separation protocol (Aitken, 1998) in Physical Research Laboratory, Ahmedabad. 20-24 aliquots of each sample were measured using Risoe TL-OSL reader in Physical Research Laboratory, Ahmedabad. The Equivalent dose (De) for each sample was measured using the OSL Double SAR (Single Aliquot Regenerative) protocol (Roberts, 2007). The Double-SAR protocol was used to surpass the luminescence signal from tiny feldspar inclusions within individual quartz grains (Cf. Fig. 5a). Test doses for samples SD/P01-P05 were set between 40 to 120 Gy (Fig.5b), while the test dose for sample SD/P06 were ranging 8-15 Gy. The aliquots were considered for ED estimation only if: (i) recycling ratio was within 1±0.1, (ii) ED error was less than 20%, (iii) test dose error was less than 10%, and (iv) recuperation was below 5% of the natural. As all the samples show over-dispersion value < 20%, we used Central Age Model (CAM) to estimate Equivalent Dose (De) (Bailey and Arnold, 2006) (Table 1; Fig. 5c).

The dose rate was estimated using online software DRAC (Durcan et al., 2015) from the data of Uranium (U), Thorium (Th), and Potassium (K) measured using α, β, and γ counters (Table 1). The estimation of moisture content was done using the fractional difference of saturated vs. unsaturated sample weight (Table 1).

3.3. Sediment analysis

We sampled the same sand layers which were used for OSL sampling. Samples were dried in a hot-air oven at 50˚C to achieve complete dryness. And then, ~2 kg of each sample were used for sedimentological analysis.

3.3.1. Sediment grain-size analysis

Each sample was dry-sieved using 1000 µm, 750 µm, 300 µm, 250 µm, 125 µm and 50 µm test sieves. Sediments above 1000 µm (very coarse-gravelly sand) and below 50 µm (silt) were discarded as we wanted to quantify the coarse-grained to very fine-grained fraction of sand (Table 2a). In figure 6a, the sediment grain-size distribution (by weight %) for the samples are plotted against φ values, which represent the size of the mesh. A higher φ value indicates a smaller grain-size. The choice of mesh follows the convention of >1000 µm (granular sand, φ ~-2 to -1), 750-1000 µm (very coarse-grained, φ~-1-0), 300-750 µm (coarse-grained, φ=0-1), 150-300 µm (medium-grained, φ=1-2), 90-150 µm (fine-grained, φ=2-3) and 50-90 µm (very fine-grained, φ=3-4).

3.3.2. Grain roundness

We performed the coning and quartering method several times with the initial mass to finalize 100g of each sample for sediment shape analysis. We separated the quartz grains from the mix by Frantz isodynamic magnetic separator and used quartz as the index grain. Grain-shape was calculated using Powers roundness index (Powers, 1953), where roundness is given by the formula-

$$Roundness = r/R \qquad \text{(Equation 1)}$$

Here, r = radius of the smallest inscribed circle within the grain and R = radius of the largest inscribed circle within the grain. We made 20 discs of each sample and measured the r and R of at least 20 grains per disc using a scaled Leica microscope. So, the minimum number of counts per sample is 120. The higher the roundness index, the more rounded the grains are. Grain-shape analysis results are provided in Fig.6b. Results of the sedimentological analysis are listed in Table 2.

4. Results

4.1. OSL chronology

Sample SD/P01 and SD/P02, taken from the base of the valley-fill, show depositional ages of 18.8±0.9 ka and 17.2±0.9 ka, respectively (Table 1). Samples SD/P03 and SD/P04, taken from the middle of the valley-fill, portrays depositional ages of 15.9±1.6 ka and 14.3±1.7 ka, respectively. Sample SD/P05 taken near the top of the valley-fill (beneath the hillslope colluvium) provides an age of 11.3±1.3 ka. Sample SD/P06 from the fine sand layer exposed in terrace T5, near the riverbed, returns a depositional age of 2.6±0.2 ka.

4.2. Sediment analysis

The samples collected from the valley-fill stored in the study area show large variations in the shape and size of the sand grains from the bottom to the top of the sediment log (Table 2). Samples SD/P01 and SD/P02, collected from the bottom of the log show a high mean grain-size (φ ~0-1); whereas, samples SD/P03 and SD/P04, taken from the middle of the log, yield a lower mean grain-size (φ~2-3) and samples SD/P05 and SD/P06 yield even smaller mean grain-size (φ~3) (Fig.6a). Similarly, the roundness coefficient (according to equation 1, described in section 3.3.2) varies from 0.27±0.08 to 0.60±0.07 (Table 2). The sample SD/P01 has the lowest roundness (0.27±0.08), and sample SD/P05 has the highest roundness (0.60±0.07), while sample SD/P06 has an approximately similar roundness value of 0.55±0.14.

5. Discussion

In this section, we compiled our field observation, chronological and sedimentological analysis of the aggraded sediments and compared our results with a previously-published record of glacial dynamics in the upper Chenab valley to assess the potential role of deglaciation in sediment aggradation observed in the Padder valley.

5.1. Sediment architecture and aggradation history

The Padder valley records ~90-100m thick sedimentary valley-fill (Fig.3b, 4a). The valley-fill units vary in grain-size ranging from fine silt to boulders having diameter~ 1m (Fig.4b). We observe an overall decrease in the clasts' size in conglomeratic layers from the bottom to the top of the litholog (Fig.4a). The lower and the middle part of the litholog are dominated by angular, poorly-sorted boulders, pebbles and gravels (Fig.4b, 4c). The clasts are coming from Higher Himalayan crystallines and high-grade metasediments. However, there is a occasional presence of more than 2m-thick silt and sandy-silt layers. The sand layers are relatively less prominent (Fig.4a). This sediment sequence is recognized as typical glacial outwash deposits (e.g., Maizels, 2002). We also found several isolated 1-1.5m thick sand layers all through the sedimentary succession and extracted quartz from the sampled sand layers for OSL dating. The lower part of the valley fills show depositional age of ~17-19 ka (age of samples- SD/P-01: 18.8±0.9 ka and SD/P-02: 17.2±0.9 ka) (Fig.4a, Table 1). In the middle of the litholog, the depositional age is ~13-17 ka (age of samples- SD/P-03: 15.9±1.6 ka and SD/P-04: 14.3±1.7 ka). The topmost sample SD/P-05 taken from a ~1m thick sand layer between two well-polished and well-rounded pebble-boulder conglomerate layers yield depositional age of ~11.3±1.3 ka (Fig.4d). The sediment sequence is topped by angular, poorly-sorted hillslope debris originated from the steep valley walls of the surrounding Lesser Himalayan units. In short, the Padder valley records net sediment aggradation during ~19-11 ka period. The transiently-stored sediments are re-incised since then. The episodic re-incision is recorded by the formation of fluvial fill terraces along the Chenab River. The lowest terrace T5 (Fig.3a) records a ~4m thick fine sand layers. The sand layer is devoid of any recognizable laminations, the grain-size is lower and the sorting is higher than fluvioglacial sand samples (Fig.6a). The equivalent dose estimates from sample SD/P-06 are also clustered, having low over-dispersion value (OD ~ 6%, cf. Table 1), suggesting a uniformly well-bleached sample. We interpret the sand layer as an aeolian deposit. This kind of aeolian deposit is common in the arid western Himalaya (e.g. Kumar et al., 2017). Aeolian activity in the Padder valley is late Holocene (age-SD/P-06: 2.6±0.2 ka).

5.2. Sediment characteristics impacted by distance from the source

Grain-size distribution and grain shape analysis of sampled sand layers from the aggraded sediment sequence show a systematic change in sediment characteristics with time. Grain-size analysis portrays a fining-upward sequence (Fig.4a), while the average roundness of the grains also increases from the bottom to the top (Fig.4b). Fig.4b illustrates a linear correlation between mean population grain-size and mean roundness co-efficient. It highlights that with time, the grain-size and angularity of grains have reduced simultaneously. We propose that the fluvioglacial sediment sequence recorded more fluvial transport with time. The lower units, which have lower roundness and coarser grain-size depict a shorter transport distance. In contrast, the upper units have higher roundness and smaller grain-size portray longer fluvial transport. So, in other words, we propose that the distance between the source of the sediments and the sediment archive has increased between 19 to 11 ka.

As the depositional attributes clearly point out a glacial source of sediments, we looked at studies on the past glacial extent in the upper Chenab valley. Eugster et al., (2016) estimated the glacial extent along the upper Chenab valley with surface-exposure dating of glacially-polished bedrocks using ^{10}Be. That study argued that ~20 ka, the valley glaciers advanced at least until ~2450 m above msl and only ~90 km upstream from the Padder valley (see point G1 in Fig.1 and Fig.2). Whereas, in the next ~5 kyr, the valley glacier retreated ~180 km and was at point G4 (~4150 m above msl) (Fig.1 and Fig.2). We propose that a similar glacial retreat must have been observed in the northern tributaries originating from the arid Zanskar Range (Fig.1). The study by Eugster et al., (2016) highlights that the significant deglaciation initiated post 20 ka and continued until the early Holocene. Our results of sediment chronology (aggradation during 19-11 ka period) and sediment grain analysis further support the glacial origin of the valley-fill sediments. Therefore, these glacial outwash deposits would show an increasing distance of the source, or in other words, increasing fluvial transport with time. Our data promptly records the signature of glacial retreat in the sediment archive.

5.3. Global climate vs. sediment aggradation in Padder valley

We compared sediment aggradation episode with previously-published climate proxies to test whether our results comply with global or regional changes in climatic intensity. In Fig.7, we show the global sea-level change curve (Lambeck et al., 2014) and Northern Hemisphere summer (August) solar insolation data at 30°N (Huybers, 2006). Lowering of global sea-level has been attributed to phases of extensive glaciation (e.g., Lambeck et al., 2002; Camoin et al., 2004). On the other hand, post-LGM (Last Glacial Maximum) sea-level rise caused by deglaciation and resulting meltwater pulses have been recorded worldwide (e.g., Lambeck and Chappel, 2001; Peltier, 2002; Harrison et al., 2019). Variations in the summer solar insolation pattern also define the glacial-interglacial phases (e.g., Gao et al., 2012). We observe that the timing of sediment aggradation in the Padder valley correlates well with the timing of the transition from the glacial (LGM) to the interglacial phase. The globally-accepted duration of the LGM is ~26-19 ka (Clark et al., 2009). Although there exist some chronological ambiguities for post-LGM deglaciation from the Himalaya, by assessing the process and analytical uncertainties of our dating method and previously-published chronological constraints on glacial fluctuations in upper Chenab valley (Eugster et al., 2016), we propose that the aggradation resulted from post-LGM deglaciation caused by global as well as a regional temperature change. We acknowledge that the post-LGM deglaciation is coupled with late Pleistocene increased monsoon intensity (e.g., Gebregiorgis et al., 2016). The impact of increased monsoon in semi-arid to arid sectors of the Himalaya (present-day mean annual rainfall< 1m/y) is yet to be verified. However, by looking at the grain-size variation in the sediment archive, we may well favor that the Padder valley probably had an insignificant influence of monsoon strengthening, as the early Holocene sediments are of smaller grain-size in comparison to the sediments from below. Strong monsoon in early Holocene would have reflected higher discharge and increased stream power, ultimately increasing the grain-size of sediments.

5.4. Minimum stored volume of sediments and erosional flux

We estimated the minimum stored volume of sediment archive at the end of aggradation using the relicts of T1 terrace level as the upper bound and the T0 (River-level) as the lower bound. We extrapolated the possible upper surface of the sediment archive by 'kriging' 3D interpolation technique in ArcGIS. We used the denuded bedrock valley walls as the lateral limits of the archive. At the basin high-stand, the calculated minimum volume is 0.5-0.6 km^3. Assuming an average sediment density to be 2200 kg/m^3, the minimum stored mass would be ~120-140 Mt. However, at present, only 30-35% of the sediment volume is remaining. The rest of the transiently-stored mass has been remobilized by episodic incision during Holocene, leaving behind river-cut terraces.

5.5. Regional significance of our study

Sediment aggradation and re-incision in a majority of the NW Himalayan valleys since the late Pleistocene have been attributed to fluctuations in climate forcing- for example, Sutlej valley (Bookhagen et al., 2005), Kangra valley (Dey et al., 2016); Zanskar valley (Chahal et al., 2019); Goriganga valley (Ali et al., 2013), Baspa valley (Dutta et al., 2018), Spiti valley (Srivastava et al., 2013), Ganga valley (Dutta et al., 2012), Bhagirathi valley (Barnard et al., 2004), Alakananda valley (Juyal et al., 2010; Ray and Srivastava, 2010), Garhwal region (Scherler et al., 2015), etc. Nearly all the studies have documented valley aggradation by ~100m thick fluvial and/or fluvioglacial sediments. However, it is tricky to decouple the monsoon-influenced and deglaciation-influenced aggradation during the post-LGM to early Holocene period. It is understood that the drainage systems that lie in the foreland-ward side of the main orographic barrier have a greater influence of the Indian Summer Monsoon and therefore, the valley aggradation is attributed to transient increase in sediment supply driven by enhancement of monsoon rainfall ~16-10 ka (e.g., Bookhagen et al., 2005; Dey et al., 2016). However, studies by Barnard et al., (2004), Kumar and Srivastava (2017) and Dutta et al., (2018) propose that Indian Summer Monsoon can play a key role in sediment aggradation even in glacier-dominated catchments lying in the arid hinterland-ward side of the orographic barrier. In our case, the extensive hillslope debris overlying the fluvioglacial deposits may hint towards an increased hillslope sediment flux triggered by the strong monsoon in the early Holocene. Unfortunately, we do not have strong constraints on monsoon influence. To summarize, this study explores the role of deglaciation in sediment aggradation in an arid and glaciated catchment in the interiors of the Kashmir Himalaya. At the same time, it highlights how glacial retreat can be traced by examining an outwash sediment archive.

6. Conclusions

The characteristics and depositional ages of the valley-fill sediments document net aggradation in Padder valley by fluvioglacial, fluvial and partly by aeolian sediments. The main findings of our study are as follows-

a. There is a net aggradation in the valley which continued at least for the ~19-11 ka period corroborating with the commonly-observed aggradation in several other Himalayan valleys from post-LGM till early Holocene.
b. The valley-fill (~100m) mainly comprises of fluvially-transported glacial debris. The increasing roundness and reducing mean grain-size from the bottom to the top of the valley-fill suggest a gradual increase in fluvial transport with time. The sedimentary units at the base of the section reflect very short fluvial transport post deglaciation.
c. ^{10}Be exposure ages from glacially-carved bedrock surfaces suggest that during ~20-15 ka period, the main Chenab glacier retreated ~180 km. Our observation on aggraded sediments corroborate with the glacial retreat history as we see more fluvial influence on the sediments.

Our study is probably the first instance of sediment chronology from the much-underworked middle-upper Chenab valley in Jammu-Kashmir Himalaya and it highlights the role of deglaciation in sediment transport from high mountain areas in response to climate change.

Acknowledgments

S. Dey is supported by DST-INSPIRE faculty research grant by the Department of Science and Technology, India (grant #DST/INSPIRE/04/2017/003278). Authors acknowledge the help from C. Singh, S. Das and A. Das during the fieldwork. We thank A. Banerjee (IISER Pune) for his thoughts and insightful discussions.

References

Aitken, M.J., 1998. Introduction to optical dating: the dating of Quaternary sediments by the use of photon-stimulated luminescence. Clarendon Press.

Ali, S. N., Biswas, R. H., Shukla, A. D., & Juyal, N. (2013). Chronology and climatic implications of Late Quaternary glaciations in the Goriganga valley, central Himalaya, India. Quaternary Science Reviews, 73, 59-76.

Bailey, R.M. and Arnold, L.J., 2006. Statistical modelling of single grain quartz De distributions and an assessment of procedures for estimating burial dose. *Quaternary Science Reviews*, *25*(19-20), pp.2475-2502.

Barnard, P. L., Owen, L. A., & Finkel, R. C. (2004). Style and timing of glacial and paraglacial sedimentation in a monsoon-influenced high Himalayan environment, the upper Bhagirathi Valley, Garhwal Himalaya. Sedimentary Geology, 165(3-4), 199-221.

Barnard, P. L., Owen, L. A., Finkel, R. C., & Asahi, K. (2006). Landscape response to deglaciation in a high relief, monsoon-influenced alpine environment, Langtang Himal, Nepal. Quaternary Science Reviews, 25(17-18), 2162-2176.

Blöthe, J. H., Munack, H., Korup, O., Fülling, A., Garzanti, E., Resentini, A., & Kubik, P. W. (2014). Late Quaternary valley infill and dissection in the Indus River, western Tibetan Plateau margin. Quaternary Science Reviews, 94, 102-119.

Bookhagen, B., & Burbank, D. W. (2006). Topography, relief, and TRMM-derived rainfall variations along the Himalaya. Geophysical Research Letters, 33(8).

Bookhagen, B., Fleitmann, D., Nishiizumi, K., Strecker, M. R., & Thiede, R. C. (2006). Holocene monsoonal dynamics and fluvial terrace formation in the northwest Himalaya, India. Geology, 34(7), 601-604.

Bookhagen, B., Thiede, R. C., & Strecker, M. R. (2005). Late Quaternary intensified monsoon phases control landscape evolution in the northwest Himalaya. Geology, 33(2), 149-152.

Camoin, G. F., Montaggioni, L. F., & Braithwaite, C. J. R. (2004). Late glacial to post glacial sea levels in the Western Indian Ocean. Marine Geology, 206(1-4), 119-146.

Chahal, P., Kumar, A., Sharma, C. P., Singhal, S., Sundriyal, Y. P., & Srivastava, P. (2019). Late Pleistocene history of aggradation and incision, provenance and channel connectivity of the Zanskar River, NW Himalaya. Global and Planetary Change, 178, 110-128.

Clark, P.U., Dyke, A.S., Shakun, J.D., Carlson, A.E., Clark, J., Wohlfarth, B., Mitrovica, J.X., Hostetler, S.W. and McCabe, A.M., 2009. The last glacial maximum. science, 325(5941), pp.710-714.

Cunningham, A. C., & Wallinga, J. (2012). Realizing the potential of fluvial archives using robust OSL chronologies. *Quaternary Geochronology*, *12*, 98-106.

Dey, S., Thiede, R.C., Schildgen, T.F., Wittmann, H., Bookhagen, B., Scherler, D., Jain, V. and Strecker, M.R., 2016. Climate-driven sediment aggradation and incision since the late Pleistocene in the NW Himalaya, India. Earth and Planetary Science Letters, 449, pp.321-331.

Dosseto, A., Vigier, N., Joannes-Boyau, R. C., Moffat, I., Singh, T., & Srivastava, P. (2015). Rapid response of silicate weathering rates to climate change in the Himalaya.

Durcan, J.A., King, G.E. and Duller, G.A., 2015. DRAC: Dose Rate and Age Calculator for trapped charge dating. *Quaternary Geochronology*, *28*, pp.54-61.

Dutta, S., Mujtaba, S. A. I., Saini, H. S., Chunchekar, R., & Kumar, P. (2018). Geomorphic evolution of glacier-fed Baspa Valley, NW Himalaya: record of Late Quaternary climate change, monsoon dynamics and glacial fluctuations. Geological Society, London, Special Publications, 462(1), 51-72.

Dutta, S., Suresh, N., & Kumar, R. (2012). Climatically controlled Late Quaternary terrace staircase development in the fold-and-thrust belt of the Sub Himalaya. Palaeogeography, Palaeoclimatology, Palaeoecology, 356, 16-26.

Eugster, P., Scherler, D., Thiede, R. C., Codilean, A. T., & Strecker, M. R. (2016). Rapid Last Glacial Maximum deglaciation in the Indian Himalaya coeval with midlatitude glaciers: New insights from 10Be-dating of ice-polished bedrock surfaces in the Chandra Valley, NW Himalaya. Geophysical Research Letters, 43(4), 1589-1597.

Fan, Q., Lai, Z., Long, H., Sun, Y., & Liu, X. (2010). OSL chronology for lacustrine sediments recording high stands of Gahai Lake in Qaidam Basin, northeastern Qinghai–Tibetan Plateau. Quaternary Geochronology, 5(2-3), 223-227.

Fuchs, M., & Lang, A. (2001). OSL dating of coarse-grain fluvial quartz using single-aliquot protocols on sediments from NE Peloponnese, Greece. *Quaternary Science Reviews*, *20*(5-9), 783-787.

Gao, L., Nie, J., Clemens, S., Liu, W., Sun, J., Zech, R., & Huang, Y. (2012). The importance of solar insolation on the temperature variations for the past 110 ka on the Chinese Loess Plateau. Palaeogeography, Palaeoclimatology, Palaeoecology, 317, 128-133.

Gebregiorgis, D., Hathorne, E. C., Sijinkumar, A. V., Nath, B. N., Nürnberg, D., & Frank, M. (2016). South Asian summer monsoon variability during the last∼ 54 kas inferred from surface water salinity and River runoff proxies. Quaternary Science Reviews, 138, 6-15.

Harrison, S., Smith, D. E., & Glasser, N. F. (2019). Late Quaternary meltwater pulses and sea level change. Journal of Quaternary Science, 34(1), 1-15.

Hu, G., Yi, C. L., Zhang, J. F., Liu, J. H., & Jiang, T. (2015). Luminescence dating of glacial deposits near the eastern Himalayan syntaxis using different grain-size fractions. Quaternary Science Reviews, 124, 124-144.

Huybers, P. (2006). Early Pleistocene glacial cycles and the integrated summer insolation forcing. Science, 313(5786), 508-511.

Joussain, R., Colin, C., Liu, Z., Meynadier, L., Fournier, L., Fauquembergue, K., Zaragosi, S., Schmidt, F., Rojas, V. and Bassinot, F., 2016. Climatic control of sediment transport from the Himalayas to the proximal NE Bengal Fan during the last glacial-interglacial cycle. Quaternary Science Reviews, 148, pp.1-16.

Juyal, N., Sundriyal, Y., Rana, N., Chaudhary, S., & Singhvi, A. K. (2010). Late Quaternary fluvial aggradation and incision in the monsoon-dominated Alaknanda valley, Central Himalaya, Uttrakhand, India. *Journal of Quaternary Science*, *25*(8), 1293-1304.

Kothyari, G. C., Shukla, A. D., & Juyal, N. (2017). Reconstruction of Late Quaternary climate and seismicity using fluvial landforms in Pindar River valley, Central Himalaya, Uttarakhand, India. Quaternary International, 443, 248-264.

Kulkarni, A. V., Bahuguna, I. M., Rathore, B. P., Singh, S. K., Randhawa, S. S., Sood, R. K., & Dhar, S. (2007). Glacial retreat in Himalaya using Indian remote sensing satellite data. Current science, 69-74.

Kumar, A., & Srivastava, P. (2017). The role of climate and tectonics in aggradation and incision of the Indus River in the Ladakh Himalaya during the late Quaternary. Quaternary Research, 87(3), 363.

Kumar, A., Srivastava, P., & Meena, N. K. (2017). Late Pleistocene aeolian activity in the cold desert of Ladakh: a record from sand ramps. Quaternary international, 443, 13-28.

Lai, Z., Kaiser, K., & Brückner, H. (2009). Luminescence-dated aeolian deposits of late Quaternary age in the southern Tibetan Plateau and their implications for landscape history. Quaternary Research, 72(3), 421-430.

Lambeck, K., & Chappell, J. (2001). Sea level change through the last glacial cycle. Science, 292(5517), 679-686.

Lambeck, K., Rouby, H., Purcell, A., Sun, Y., & Sambridge, M. (2014). Sea level and global ice volumes from the Last Glacial Maximum to the Holocene. Proceedings of the National Academy of Sciences, 111(43), 15296-15303.

Lambeck, K., Yokoyama, Y., & Purcell, T. (2002). Into and out of the Last Glacial Maximum: sea-level change during Oxygen Isotope Stages 3 and 2. Quaternary Science Reviews, 21(1-3), 343-360.

Long, H., Lai, Z., Wang, N., & Zhang, J. (2011). A combined luminescence and radiocarbon dating study of Holocene lacustrine sediments from arid northern China. Quaternary Geochronology, 6(1), 1-9.

Maizels, J. (2002). Sediments and landforms of modern proglacial terrestrial environments. In Modern and past glacial environments (pp. 279-316). Butterworth-Heinemann.

Meetei, L. I., Pattanayak, S. K., Bhaskar, A., Pandit, M. K., & Tandon, S. K. (2007). Climatic imprints in Quaternary valley fill deposits of the middle Teesta valley, Sikkim Himalaya. Quaternary International, 159(1), 32-46.

Mehta, M., Majeed, Z., Dobhal, D. P., & Srivastava, P. (2012). Geomorphological evidences of post-LGM glacial advancements in the Himalaya: a study from Chorabari Glacier, Garhwal Himalaya, India. Journal of earth system science, 121(1), 149-163.

Meigs, A., Krugh, W. C., Davis, K., & Bank, G. (2006). Ultra-rapid landscape response and sediment yield following glacier retreat, Icy Bay, southern Alaska. Geomorphology, 78(3-4), 207-221.

Milankovich, M. (1941). Canon of insolation and the Ice-Age problems. R. Serbian Acad. Spec. Publ, 132.

Panda, S., Kumar, A., Das, S., Devrani, R., Rai, S., Prakash, K., & Srivastava, P. (2020). Chronology and sediment provenance of extreme floods of Siang River (Tsangpo-Brahmaputra River valley), northeast Himalaya. Earth Surface Processes and Landforms, 45(11), 2495-2511.

Peltier, W. R. (2002). On eustatic sea level history: Last Glacial Maximum to Holocene. Quaternary Science Reviews, 21(1-3), 377-396.

Powers, M.C., 1953, A new roundness scale for sedimentary particles: Journal of Sedimentary Petrology, 23:117-119.

Pratt-Sitaula, B., Burbank, D. W., Heimsath, A., & Ojha, T. (2004). Landscape disequilibrium on 1000–10,000 year scales Marsyandi River, Nepal, central Himalaya. Geomorphology, 58(1-4), 223-241.

Rashid, I., Romshoo, S. A., & Abdullah, T. (2017). The recent deglaciation of Kolahoi valley in Kashmir Himalaya, India in response to the changing climate. Journal of Asian Earth Sciences, 138, 38-50.

Ray, Y., & Srivastava, P. (2010). Widespread aggradation in the mountainous catchment of the Alaknanda–Ganga River System: timescales and implications to Hinterland–foreland relationships. Quaternary Science Reviews, 29(17-18), 2238-2260.

Scherler, D., Bookhagen, B., Wulf, H., Preusser, F., & Strecker, M. R. (2015). Increased late Pleistocene erosion rates during fluvial aggradation in the Garhwal Himalaya, northern India. Earth and Planetary Science Letters, 428, 255-266.

Sharma, S., Chand, P., Bisht, P., Shukla, A. D., Bartarya, S. K., Sundriyal, Y. P., & Juyal, N. (2016). Factors responsible for driving the glaciation in the Sarchu Plain, eastern Zanskar Himalaya, during the late Quaternary. Journal of Quaternary Science, 31(5), 495-511.

Singh, A. K., Pattanaik, J. K., & Jaiswal, M. K. (2017). Late Quaternary evolution of Tista River terraces in Darjeeling-Sikkim-Tibet wedge: Implications to climate and tectonics. Quaternary International, 443, 132-142.

Sinha, S., Suresh, N., Kumar, R., Dutta, S., & Arora, B. R. (2010). Sedimentologic and geomorphic studies on the Quaternary alluvial fan and terrace deposits along the Ganga exit. Quaternary International, 227(2), 87-103.

Smith, J.A., Andersen, T.J., Shortt, M., Gaffney, A.M., Truffer, M., Stanton, T.P., Bindschadler, R., Dutrieux, P., Jenkins, A., Hillenbrand, C.D. and Ehrmann, W., 2017. Sub-ice-shelf sediments record history of twentieth-century retreat of Pine Island Glacier. Nature, 541(7635), pp.77-80.

Srivastava, P., Bhakuni, S. S., Luirei, K., & Misra, D. K. (2009). Morpho-sedimentary records at the Brahmaputra River exit, NE Himalaya: Climate–tectonic interplay during the Late Pleistocene–Holocene. Journal of Quaternary Science: Published for the Quaternary Research Association, 24(2), 175-188.

Srivastava, P., Ray, Y., Phartiyal, B., & Sharma, A. (2013). Late Pleistocene-Holocene morphosedimentary architecture, Spiti River, arid higher Himalaya. International Journal of Earth Sciences, 102(7), 1967-1984.

Suresh, N., Bagati, T. N., Kumar, R., & Thakur, V. C. (2007). Evolution of Quaternary alluvial fans and terraces in the intramontane Pinjaur Dun, Sub-Himalaya, NW India: interaction between tectonics and climate change. Sedimentology, 54(4), 809-833.

Tucker, G. E., & Slingerland, R. (1997). Drainage basin responses to climate change. Water Resources Research, 33(8), 2031-2047.

Wang, Y., Cheng, H., Edwards, R.L., Kong, X., Shao, X., Chen, S., Wu, J., Jiang, X., Wang, X. and An, Z., 2008. Millennial-and orbital-scale changes in the East Asian monsoon over the past 224,000 years. Nature, 451(7182), pp.1090-1093.

Figure captions

Figure 1: (inset) An overview map of the western Himalaya showing major drainages and locations of some of the already-investigated late Pleistocene-Holocene sediment archives in the region. The notable sediment archives include the Sutlej valley (Bookhagen et al. 2005); Kangra valley (Dey et al., 2016); Goriganga valley (Ali et al., 2013), Zanskar valley (Chahal et al., 2019); Baspa valley (Dutta et al., 2018), Spiti valley (Srivastava et al., 2013), Ganga valley (Dutta et al., 2012), Bhagirathi valley (Barnard et al., 2004), Alakananda valley (Juyal et al., 2010; Ray and Srivastava, 2010), Garhwal region (Scherler et al., 2015), etc. (a) A regional topographic map showing the Chenab drainage network and present-day glacial extent (GLIMS data). Points G1-G4 marks the extent of glacial advancement during ~20-15 kyr in the upper Chenab valley (adapted from Eugster et al., 2016). (b) TRMM data (Bookhagen and Burbank, 2006) showing variations in present-day annual rainfall across a part of the western Himalaya. Note that the Padder valley receives low annual rainfall (< 1m/yr).

Figure 2: Longitudinal profile of the Chenab River within the Himalayan orogen showing glacial extent during since 20 ka marked by points G1-G4 on the profile (cf. Figure 1a). Post-LGM temperature rise have inflicted ~180 km retreat of the Chenab valley glacier. (Inset) A view of the 'U-shaped' Padder valley taken from the east of Padder-Gulabgarh town showing the steep valley-walls and fluvial terraces sculpted into fluvioglacial sediment.

Figure 3: (a) Terrace map of the Padder valley showing at least five terrace levels above the present-day Riverbed. Locations of sample collection are shown. (b) A conceptual valley-profile drawn across the Padder valley showing aggradation during late Pleistocene and episodic re-incision of the aggraded valley-fills forming Holocene fill terraces.

Figure 4: (a) Composite sediment-log and associated OSL ages of the aggraded valley-fill observed in Padder valley. Note that, the sediment record has breaks in between where proper exposures are not found. (b) Poorly-sorted angular clast-dominated sediments at the base of the succession. (c) Another pulse of glacial outwash sediments from the middle of the litholog showing lesser angularity of the clasts. (d) Well-polished, well-rounded clasts from the top of the section suggesting long fluvial transport.

Figure 5: (a) Shine curve, (b) Dose growth curve and (c) Radial plot for De estimation for sample SD/P-02. (d) Photomicrograph of sample SD/P-02.

Figure 6: (a) Grain-size distribution of sand samples showing an upward-fining sequence along the litholog. Note that, grains above 1000 μm and below 50 μm are discarded. (b) Roundness co-efficient of separated quartz grains plotted against mean grain-size shows lowering of angularity and decrease of grain-size from the bottom to the top of the litholog, suggesting an increasing fluvial transport with time.

Fig.7: Rate and duration of valley-filling plotted along with NHSI data (Huybers, 2006) and global sea-level curve (Lambeck et al., 2014). It highlights the correlation of global temperature rise at glacial to interglacial phase transition leading to glacial melting and sediment aggradation in Padder valley.

Table captions

Table 1: Sample location, elemental analysis and equivalent dose and depositional ages of sand samples (using OSL double-SAR protocol and central age model).

Table 2: (a) Details of grain-size distribution in collected samples. Note that, grains above 1000 μm and below 50 μm are discarded. (b) Mean± standard deviation of roundness co-efficient for sampled sand layers.

Figures for the manuscript titled

Post-LGM glacial retreat drives aggradation in the interiors of the Kashmir Himalaya

Saptarshi Dey, Naveen Chauhan, Anushka Vasistha and Vikrant Jain

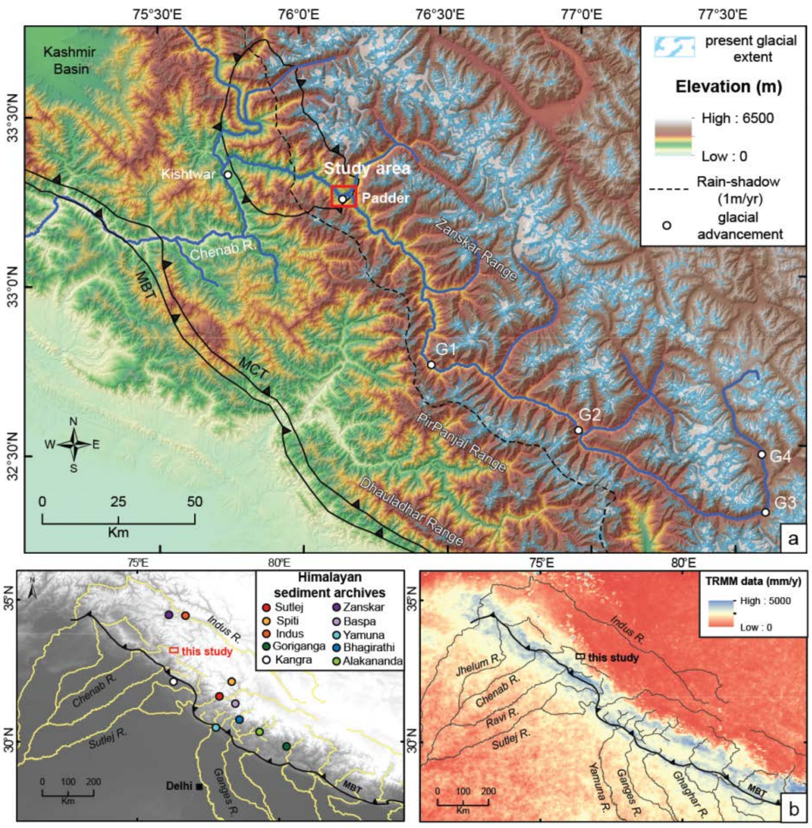

Figure 1: (inset) An overview map of the western Himalaya showing major drainages and locations of some of the already-investigated late Pleistocene-Holocene sediment archives in the region. (a) A regional topographic map showing the Chenab drainage network and present-day glacial extent (GLIMS data). Points G1-G4 marks the extent of glacial advancement during ~20-15 kyr in the upper Chenab valley (adapted from Eugster et al., 2016). (b) TRMM data (Bookhagen and Burbank, 2006) showing variations in present-day annual rainfall across a part of the western Himalaya. Note that the Padder valley receives low annual rainfall (< 1m/yr).

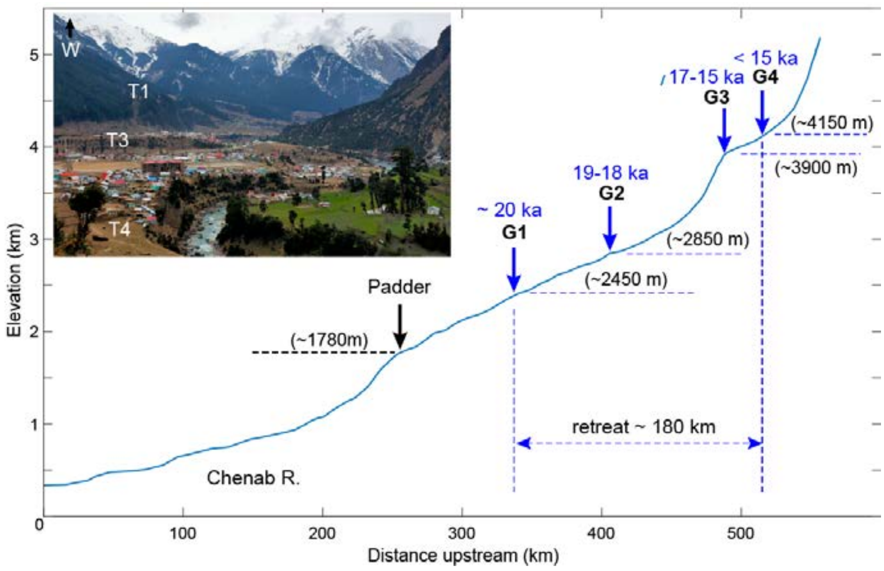

Figure 2: Longitudinal profile of the Chenab River within the Himalayan orogen showing glacial extent during since 20 ka marked by points G1-G4 on the profile (cf. Figure 1a). Post-LGM temperature rise have inflicted ~180 km retreat of the Chenab valley glacier. (Inset) A view of the 'U-shaped' Padder valley taken from the east of Padder-Gulabgarh town showing the steep valley-walls and fluvial terraces sculpted into fluvioglacial sediment.

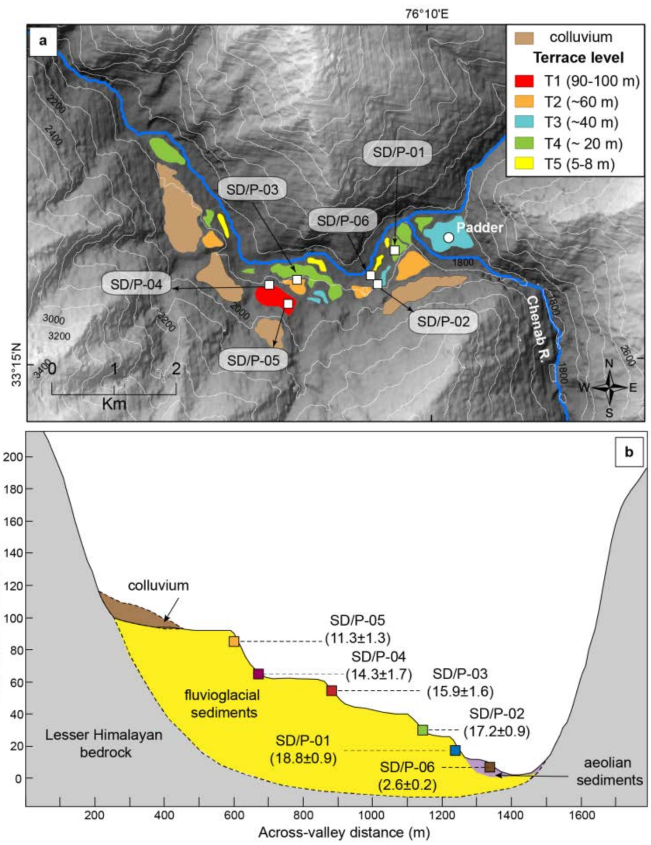

Figure 3: (a) Terrace map of the Padder valley showing at least five terrace levels above the present-day Riverbed. Locations of sample collection are shown. (b) A conceptual valley-profile drawn across the Padder valley showing aggradation during late Pleistocene and episodic re-incision of the aggraded valley-fills forming Holocene fill terraces.

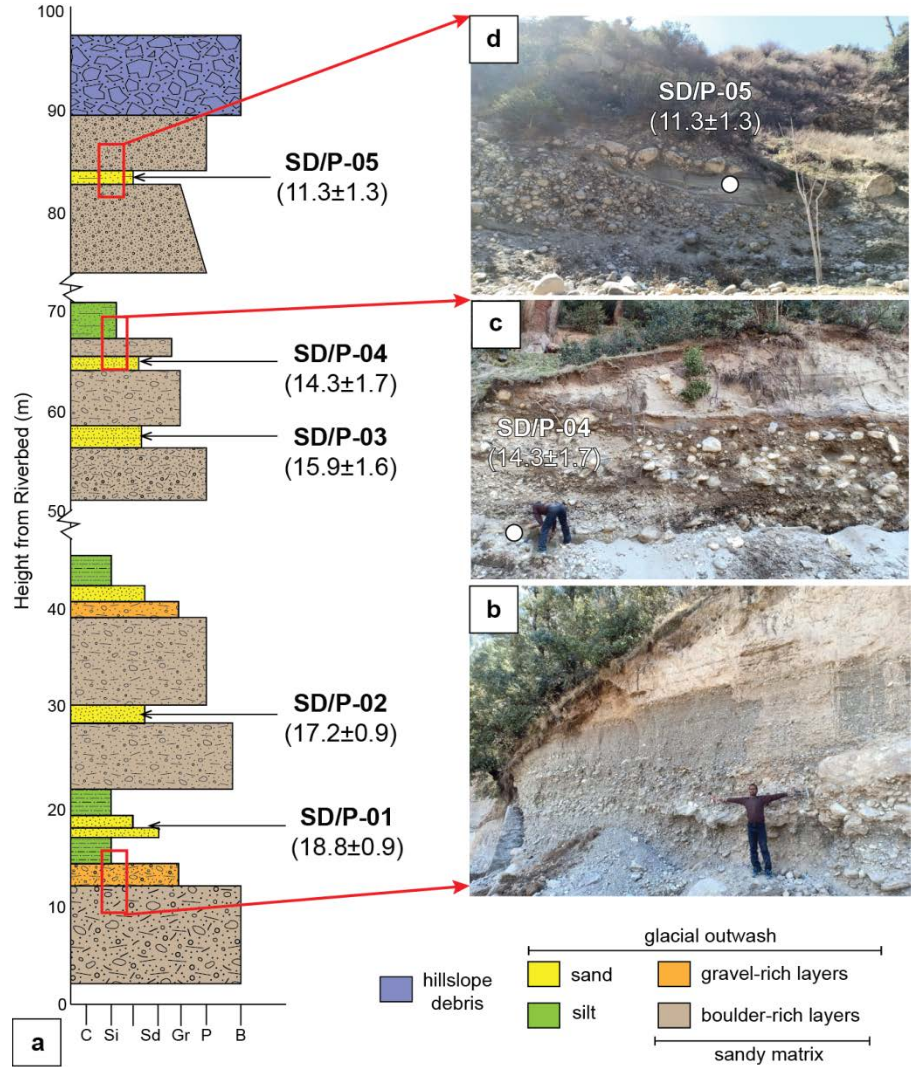

Figure 4: (a) Sediment-log and associated OSL ages of the aggraded valley-fill observed in Padder valley. Note that, the sediment record has breaks in between where proper exposures are not found. (b) Poorly-sorted angular clast-dominated sediments at the base of the succession. (c) Another pulse of glacial outwash sediments from the middle of the litholog showing lesser angularity of the clasts. (d) Well-polished, well-rounded clasts from the top of the section suggesting long fluvial transport.

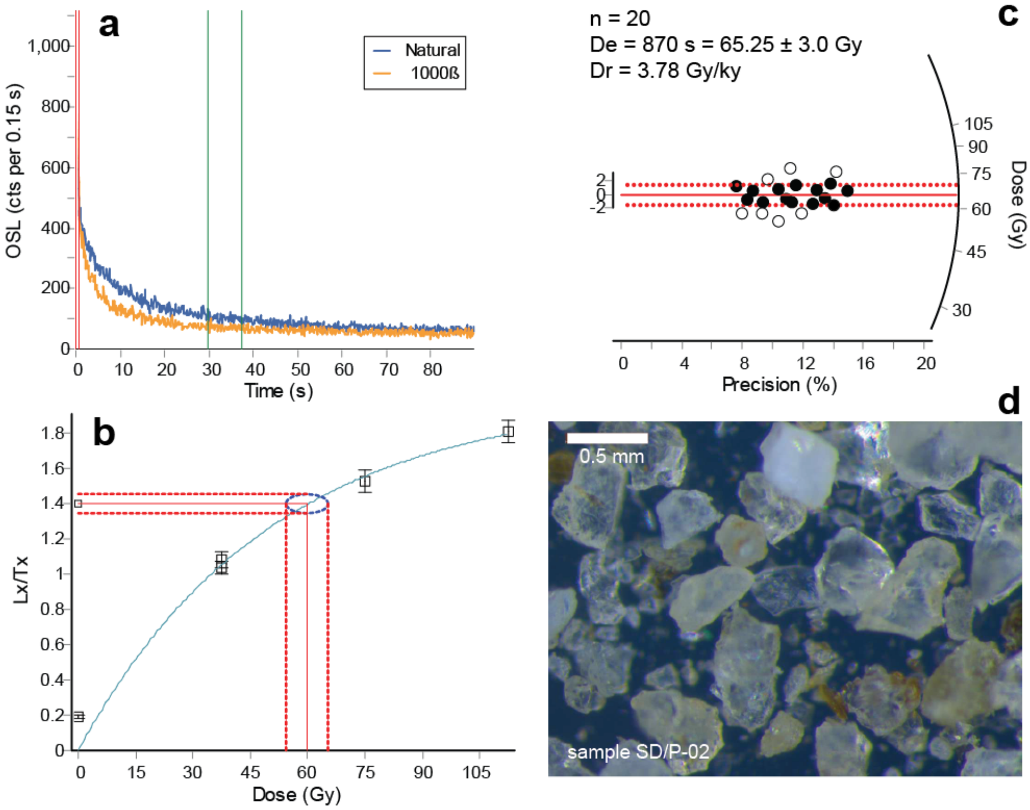

Figure 5: (a) Shine curve, (b) Dose growth curve and (c) Radial plot for De estimation for sample SD/P-02. (d) Photomicrograph of sample SD/P-02.

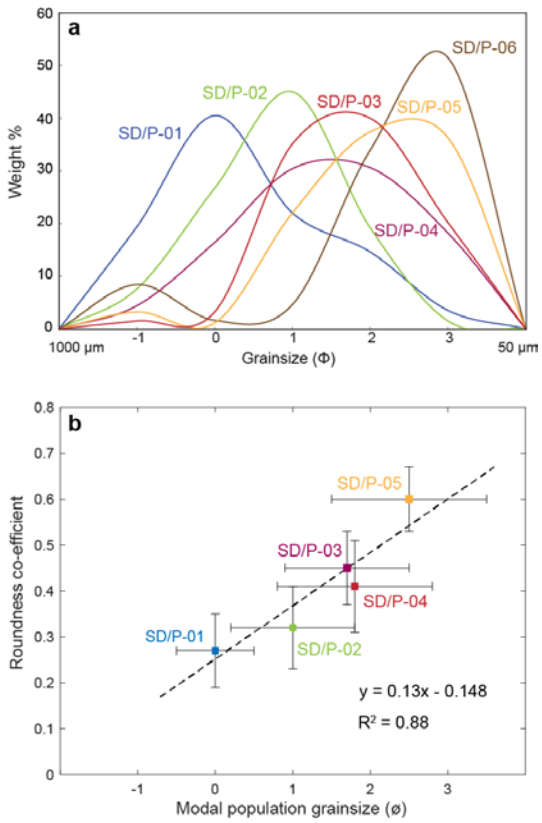

Figure 6: (a) Grain-size distribution of sand samples showing an upward-fining sequence along the litholog. Note that, grains above 1000 μm and below 50 μm are discarded. (b) Roundness co-efficient of separated quartz grains plotted against mean grain-size shows lowering of angularity and decrease of grain-size from the bottom to the top of the litholog, suggesting an increasing fluvial transport with time.

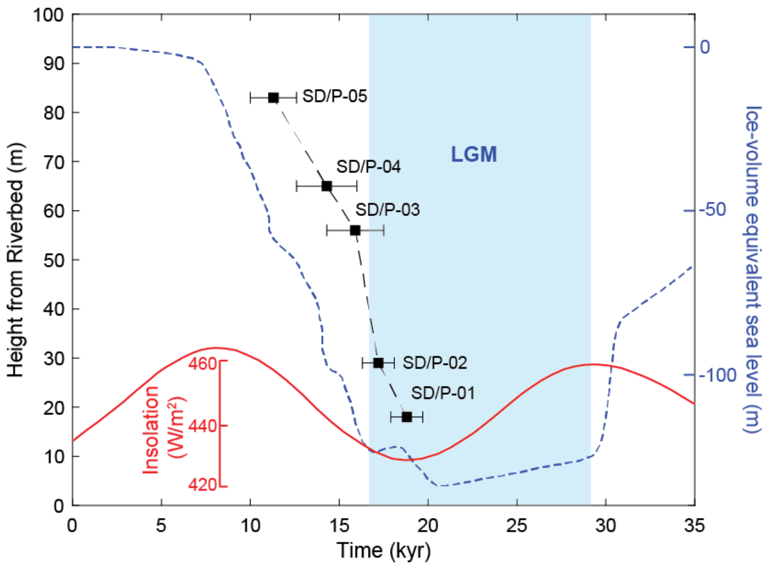

Fig.7: Rate and duration of valley-filling plotted along with NHSI data (Huybers, 2006) and global sea-level curve (Lambeck et al., 2014). It highlights the correlation of global temperature rise at glacial to interglacial phase transition leading to glacial melting and sediment aggradation in Padder valley.

Tables

Sample	Latitude (˚)	Longitude (˚)	height from River (m)	U (ppm)	Th (ppm)	K (%)	Moisture (%)	Dose rate (Gy/ky)	Paleo-dose (Gy)	OD (%)	Age (ky)
SD/P01	33.26515	76.16135	18	2.9	21	2.4	6	4.43±0.2	83±3	10.1	18.8±0.9
SD/P02	33.26198	76.15896	29	3.3	13.8	2.1	8	3.78±0.1	65±3	11.6	17.2±0.9
SD/P03	33.26187	76.13881	57	2.8	9.5	2.6	6	3.76±0.1	60±6	19.2	15.9±1.6
SD/P04	33.26141	76.13258	65	3.5	12.9	2	6	3.5±0.1	50±6	20.4	14.3±1.7
SD/P05	33.26035	76.13083	84	3.9	7.2	1.9	9	3.18±0.1	36±4	14.5	11.3±1.3
SD/P06	33.26242	76.13725	4	3.3	15.5	2.5	10	4.26±0.1	11±1	6.2	2.6±0.2

Table 1: Sample location, elemental analysis and equivalent dose and depositional ages of sand samples (using OSL double-SAR protocol and central age model).

a. Grain-size distribution

Grain type	Phi	SD/P-01	SD/P-02	SD/P-03	SD/P-04	SD/P-05	SD/P-06
vc sand	-1	19.4	7.6	1.5	4.4	3.2	8.4
c sand	0	40.5	26.7	3.2	16.4	1.1	1.6
m sand	1	22	45	35.1	30.4	22	4.6
f sand	2	14.6	19.2	40	30.6	37.4	33.9
vf sand	3	3.5	1.5	20.2	18.2	36.3	51.5

values given as weight percentage

b. Roundness co-efficient

Samples	mean	std. dev.
SD/P-01	0.27	0.08
SD/P-02	0.32	0.09
SD/P-03	0.41	0.10
SD/P-04	0.45	0.08
SD/P-05	0.60	0.07
SD/P-06	0.55	0.14

Table 2: (a) Details of grain-size distribution in collected samples. Note that, grains above 1000 µm and below 50 µm are discarded. (b) Mean± standard deviation of roundness co-efficient for sampled sand layers. Minimum number of reading per sample is 120.